The Caturo: A Sub-millimetre Diameter Glass Concentric Tube Robot with High Curvature

*Chibundo J. Nwafor**, *Guillaume J. Laurent*, *Patrick Rougeot*, and *Kanty Rabenorosoa*

FEMTO-ST Institute, Univ. Bourgogne Franche-Comté, CNRS
AS2M department
24 rue Alain Savary, 25000 Besançon, France
Email Address: [chibundo.nwafor, guillaume.laurent, patrick.rougeot, rkanty]@femto-st.fr

Keywords: *concentric tube robot, pre-curved glass tube, high curvature, kinematics, vitreoretinal surgery*

Concentric tube robots (CTRs) are considered promising in medical applications involving intracorporeal confined spaces, high dexterity, and 3D path following. Most CTRs are currently made of Nitinol due to its superelastic properties and biocompatibility. In this paper, we propose to use glass-polymer composite tubes to ease the shape setting, decrease friction, and benefit linear elasticity. The paper presents a new generation of CTR: Caturo, which is made of flexible and miniaturized sub-millimeter glass-polymer tubes. Caturo has also an unprecedented radius of curvature that reaches as low as 5 mm. It is fabricated through the thermal treatment of a thin heat-shrink polymer tube on a glass capillary in a 3D-printed mold. The fabrication process is quick, versatile, and relatively low-cost. Various free space deployment operations were demonstrated, such as 3D helical pre-curved tube deployment, conical-spiral deployment, and constrained 3D deployment through needle orifices. The forward kinematic model (FKM), inverse kinematic model (IKM), and stability analysis were experimentally validated. Finally, this paper proposes pre-curved optic fiber deployment with laser emission capability, fluid sample suction, and delivery operation. There is also a proposed vitreoretinal surgery using a fish eye under optical coherence tomography (OCT) visualization.

1 INTRODUCTION

Concentric tube robots (CTRs), referred to as active cannulas in medicine, are among the smallest members of the continuum (i.e. continuously flexible) robot family. [1,2] They comprise concentrically pre-curved tubes nested into each other (Figure 1A). Due to the arrangement of the tubes, when actuated (translation/rotation at its proximal end), the configuration of the backbone of the robot changes as the tubes elastically interact. [3] It has evolved tremendously from manual to automated systems over time; the earliest prototype was developed around 1985. This early prototype consisted of a straight outer tube and a pre-curved interior wire (the Mammalok). Eventually, this prototype progressed to a motorized version in 2005. [4] The structural component of the active part, which only has concentric tubes, makes further miniaturization possible when compared to other members of the continuum robot family (with a tendon, rod, and disk and no shape memory alloy (SMA), electroactive polymers (EAP), or pneumatic backbone actuated type of continuum robots). [1,5] Many proposed CTR applications primarily focus on clinical intervention due to CTRs' dexterity and ability to be deployed throughout hard-to-reach surgical sites, where existing straight and rigid MIS instruments are unable to reach. In fact, their inherent compliance enables them to be safely implemented into medical environments. [1,4] These proposed applications include: skull base surgery, abdominal surgery, neurosurgery, cardiac surgery, transvascular surgery, natural orifice surgery, and urological surgery, as reviewed in [5, 6]. Most proposed applications of CTRs are still exclusively used for medical interventions. However, these applications could also be used outside of medicine.

The design and fabrication of CTR tubes over the years has depended on Nitinol. Nitinol is flexible, with elastic strain that can reach 8-11%; it has super-elasticity, which makes it possible to be pre-curved into any given shape through heat setting. [1,7] The Nitinol tube can be constrained into a desired shape or mold either with an air furnace or by electric joule heating. CTR has some technical limitations in terms of the commercially available diameters, which determine its obtainable radius of curvature. The fabrication and bending process used to pre-curve the Nitinol CTR tubes requires heating in a furnace (typically 500° for 20 minutes). A patterned engraved steel mold is used to constrain the tube in the desired shape, which may not permit patient-specific, fast, and on-site fabrication. In addition, the spring-back effect makes it difficult to precisely control the obtained curvature. The advances made in 3D additive manufacturing paved the way for the use of polymers and plastics in CTR tube prototyping. For medical applications, the possibility for on-site and direct fabrication approach constitutes a major advantage in patient-specific and procedure-specific scenarios when compared to Nitinol [7,8]. However, the tube properties depend highly on the 3D printing technology and its setting (e.g., the resolution, obtainable surface

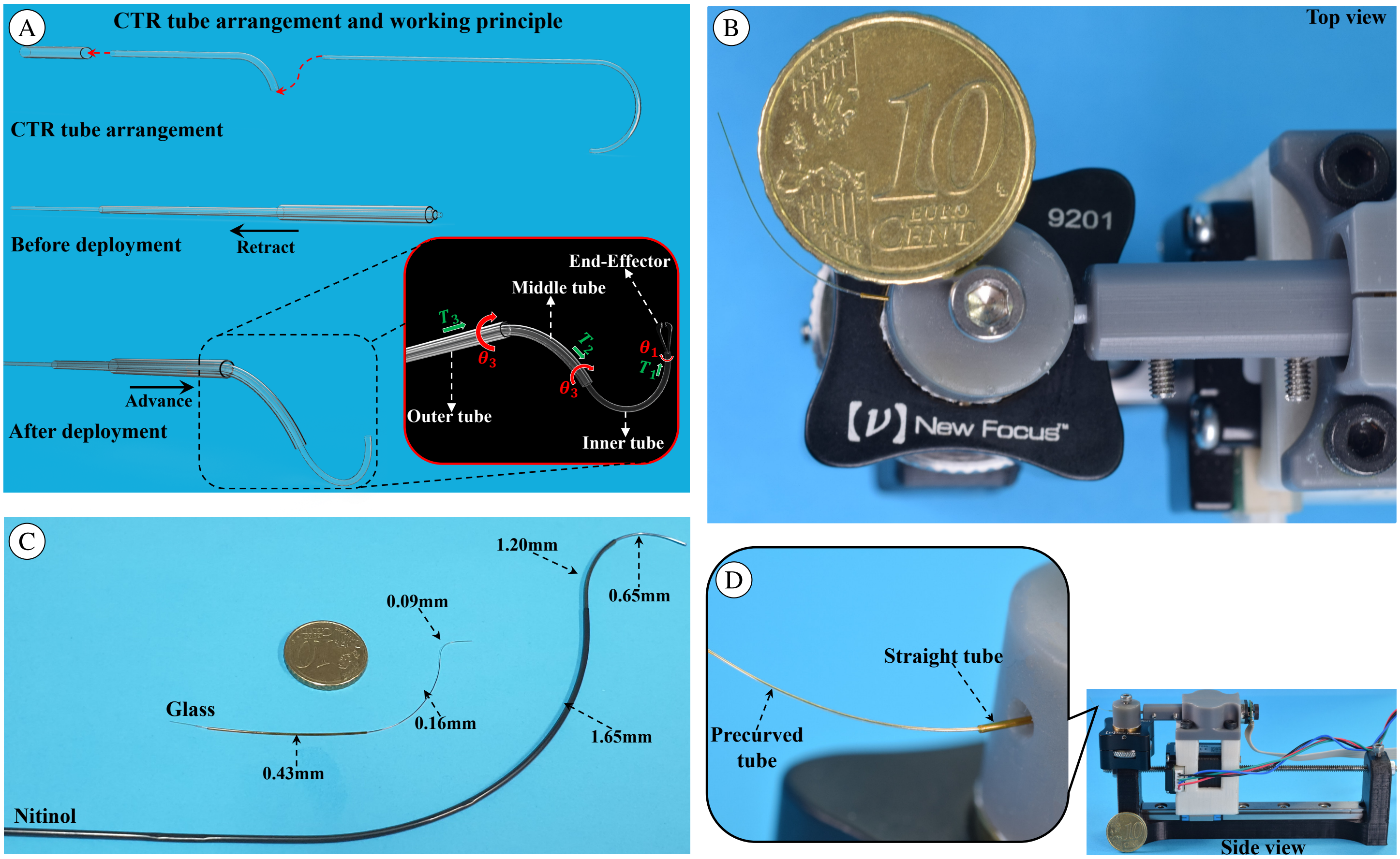

Figure 1. The Caturo: a capillary flexible CTR made of glass, with a high curvature and a sub-millimetric diameter. A) Arrangement of CTR tubes considering the case of dominance stiffness pair, where the inner tube that is characterized by a smaller diameter and less stiffness is inserted and conforms to the shape of the larger and thicker outer tubes, represented as "Before deployment". During the deployment operation, each individual tube morphs into its original pre-curved shape as the robot takes its final configuration, represented as "After deployment". **B)** A robotized two-tube Caturo, with sub-millimeter diameters (0.16mm & 0.35mm) and a very low radius of curvature (11.5mm), during a deployment. **C)** A comparison of three tube CTR configurations between the conventional Nitinol material and that of the sub-millimeter glass (diameter of each tube is displayed). **D)** The actuation unit is characterized by two DoF; the outer tube is fixed to the robot base while the inner tube is attached to the linear and rotary actuation for the demonstrations in this paper.

smoothness, thickness, and available materials). [7] Both approaches have advantages and drawbacks, which range from the limits of the manufacturing techniques to the potential results (e.g., the desired mechanical properties of the material, the minimum obtainable tube diameters and curvatures). Obtaining a high curvature enables an increase in the kinematics performance, [9] but the stability level has to be managed effectively. [10,11] The robotics community is highly dependent on the use of Nitinol due to its more desirable mechanical properties (e.g., obtainable strain, miniaturization, and surface smoothness), which partially explain why it the most used material for the fabrication of the pre-curved CTR tube. Consequently, there are challenges posed by the fabrication of miniaturized, high curvature, and on-site fast customizable complex 3D CTR tube shapes.

This paper introduces a new generation of CTRs by enabling a novel approach for obtaining pre-curved CTR tubes with sub-millimeter diameters and a high curvature. This is achieved by using thin heat-shrink polymers on micro-glass capillaries to actualize the first ever sub-millimeter CTR prototype composed of glass material, as shown in Figure 1. This robot is "Caturo", which stands for a capillary tube robot with typical external tube diameters from 434μm to 90μm and an unprecedented radius of curvature as low as 5mm. Thin glass is distinct from conventional glass due to its strength and flexibility. [12,13] These inherent properties of glass on a micro-scale are beneficial in the design of miniaturized 3D structures. Figure 1 displays the compact, miniaturized, and hand-held robot prototype with an active backbone comprised of glass (Figure 1D); most of its actuation unit frame support was fabricated by a lightweight 3D printed polymer. Figure 1C highlights the scaling difference with a side-by-side comparison of a nested pre-curved tube configuration by the conventional Nitinol and a miniaturized sub-millimeter glass material. In addition to operating on such a miniaturized scale, the advantages of our approach are similar to those of 3D printed CTR. Advantages include low-cost, patient-specific capability and lower temperature in short duration requirement, which permits the use of a 3D printed mold to obtain various complex glass tube shapes.

The main contribution of this paper is to present a CTR made of glass tubes. To the best of our knowledge, this CTR has the smallest diameter range and lowest radius of curvature among all the other figures found in the literature. Multiple applications were demonstrated in order to highlight the robot's capabilities. Such capabilities have the possibility for end-effector functionalization using fluid or light-driven actuators or sensors. An additional aim of this paper is to present a new approach of fabricating pre-curved sub-millimeter CTR tubes with glass capillaries and optic fibers, by heat treatment using a heat-shrink polymer and a 3D printed mold.

2 RESULTS

2.1 Precurved Sub-millimetre Glass CTR Tubes

In CTRs, higher dexterity in a tightly confined region requires a small radius of curvature.[9] For this reason, we answer the question of whether pre-curved tubes made of glass, with a sub-millimeter diameter less than that of conventional Nitinol, can permit deployment in hard-to-reach surgical sites. The sub-millimeter tubes consist of fused silica, which was coated with a thin standard polyimide (refer to Table-1) to prevent direct glass surface exposure and provide mechanical rigidity (Polymicro Technologies). For fused silica, the presence and type of surface flaws dictate its strength rather than the strength of its Si-O bonds.[40] By using protective polymer coating, which is common in optics fiber, this stress can significantly be reduced. In addition, its mechanical strength can be further improved by minimizing the flaws in glass and enabling a low surface area.[40–42] All these factors guarantee the ability of capillary glass to withstand high deformation under bending stress. It allows the capillary glass to have flexibility similar to the optics fiber, unlike the brittle and fragile normal glass in the macro scale. Fused silica has a non-linear elastic property and the applied strain determines the elastic modulus,[43,44] with the maximum bend radius of curvature, deduced by considering tensile strength in Equation (1).

$$\sigma = E_o \frac{r_c}{r} \left[1 + \alpha \frac{r_c}{r} + \beta \left(\frac{r_c}{r} \right)^2 \right] \tag{1}$$

σ is the surface stress, E_o is Young's modulus at zero strain (70GPa), r_c is the capillary radius, and r is the bending radius of curvature. $\alpha = 2.30$ and $\beta = 8.48$ are the second order and third order nonlinear material coefficients, respectively. Considering the glass tube diameters used, the relationship between their bending stress and the obtainable radius of curvature, as derived from equation (1), is displayed in Figure 2A. Although theoretically, the ultimate tensile strength of fused silica can reach 4.83GPa (green dash line), we considered nominal bending stress of 0.69GPa (black dash line); this consideration is in line with the Polymicro poof test (Polymicro Technologies). Figure 2A explains why it was possible to obtain a small bend radius of curvature in glass (down to 5 mm for 90μm), which is very flexible to sustain bending stress below nominal value without fracture. Considering its ultimate tensile strength, the figure indicates that it can withstand more stress in cases of path contact during deployment and manipulation. For both glass and Nitinol, the precurvature limits, or the obtainable minimum radius of curvature, depend on the available tube diameter; a smaller tube diameter guarantees a smaller radius of curvature without plastic deformation. Figure 2A also demonstrated that it is theoretically possible for a 1 mm glass tube to sustain bending stress below the ultimate tensile strength. This level of bending stress can guarantee a 10 mm radius of curvature like that of Nitinol, which has a minimum radius of curvature of 15 mm (Figure 2C).

The glass tubes are commercially sold in a straight form with multiple inner and external diameters; the diameters can be customized on request. Using the thermal treatment of a thin heat-shrink polymer, known as Polyethylene terephthalate (PET), on the micro-glass capillary; pre-curved tube shapes were obtained, as shown in Figure 2B. The radius of the curvature for the fabricated micro-glass pre-curved tube can be as small as 5mm (see Supplementary A). A selection of the nested sub-millimeter planar pre-curved CTR glass tube samples is displayed in Figure 2B. The 3D helical pre-curved tubes in Figure 2B demonstrate that complex glass tube shapes can be obtained by changing the 3D printed mold design. The utility of this approach can be broadened to other

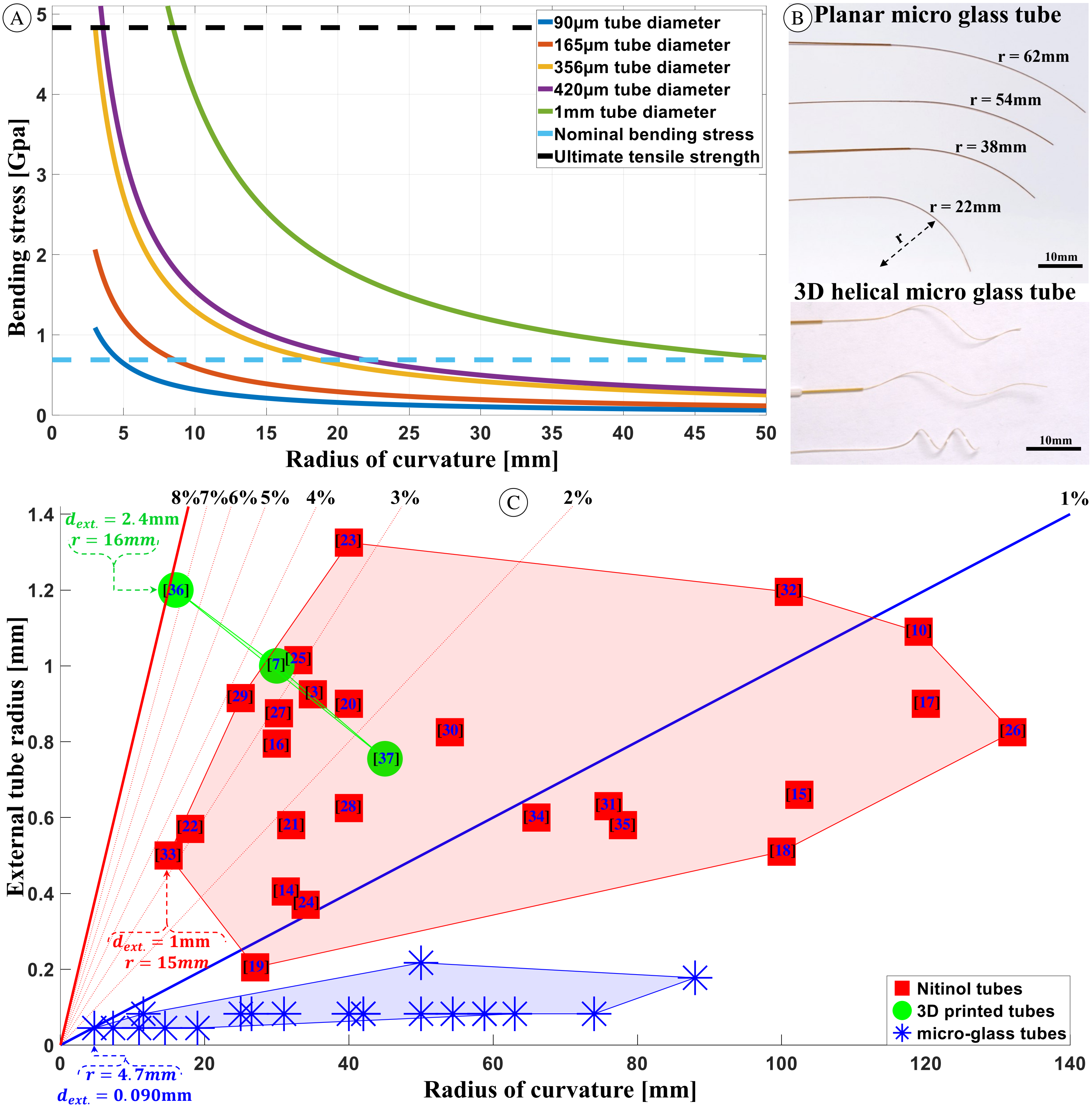

Figure 2. Sub-millimetre pre-curved glass tubes. **(A)** The relationship between the glass capillary bending stress and the obtainable bend radius of curvature for the glass diameters, **(B)** The samples of pre-curved micro-glass tubes with obtainable shapes and curvatures, such as the simple planar to complex curvatures, for various demonstrations of sub-millimeter glass tube flexibility and ability to slide into each other for possible CTR configurations. **(C)** The unprecedented region of interest we operate in when comparing all the inner smallest CTR pre-curved tubes for the prototypes in the literature. It involves the conventional Nitinol (in red marker) and 3D printed technology (in green marker) and that of the sub-millimeter glass tubes (in blue marker). The external radius and radius of curvature of the innermost tube prototypes in literature were considered. The percentage lines are the recoverable maximum strain below permanent deformation or fracture for different tubes with an average of 8% for Nitinol [38] (red solid line) and around 1% for glass [39] (blue solid line).

composite design structures. This approach can be used beyond the practice of heat shrink on micro-glass capillaries. The merit of the composite structure of the heat shrink on glass approach is that glass capillaries are sufficiently stiff. The stiffness can enable the fabrication of CTR pre-curved tube with an unprecedented diameter, unlike using polymers alone. The approach is less costly than Nitinol. Moreover, there is a benefit of reduced friction due to the lower friction coefficient between glass and PET (0.23), [45] compared to the Nitinol-on-Nitinol friction coefficient (0.3).[46,47] Full details regarding the fabrication procedure, curvature accuracy, validation, and characterization for a set of pre-curved glass tubes are detailed in the Methods/Experimental Section.

The result of the fabrication of pre-curved CTR tubes is presented in blue in Figure 2C; this figure highlights the region of interest for the Caturo by displaying the obtainable CTR tube radius of curvatures and the smallest diameter range with respect to the state-of-the-art. For CTR, the recoverable strain under deformation is one of the key factors for the flexible material. Considering a single tube, the relationship between the strain limit ϵ and radius of curvature R (without plastic deformation) in straightening a pre-curved tube is $R = r/\epsilon + r$. r is the external tube radius. Note, since ϵ is small, $r << r/\epsilon$ and therefore, $\epsilon \approx R/r$. This relationship indicates that a miniaturized tube radius could enhance dexterity and enable mobility in tighter covers. Figure 2C displays the plot of strain as a function of the external tube radius and the radius of curvature for all inner tubes of the CTR prototypes in the literature. Most of the recoverable bending strain of Nitinol is considered as 8% [38], which is represented by the straight red line in Figure 2C; this demonstrates that all the Nitinol tubes operated below the recoverable boundary. The maximum strain of fiberglass before fracture is near 1%[39], which is represented as the straight blue line in Figure 2C; it shows how the pre-curved sub-millimeter glass respected this boundary too. When comparing the pre-curved sub-millimeter glass tubes, to the smallest CTR prototype tubes in the literature (made of either Nitinol or 3D printed polymers), there were three key observations in Figure 2C. Using glass tubes to fabricate pre-curved CTR tubes with the smallest possible external diameter (∼90µm), can permit manipulation at the sub-millimeter scale. This fabrication method can allow deployment or manipulation within a very confined space, which is not as feasible for conventional CTRs (15 mm minimum radius of curvature in Figure 2C[33]). It is also possible to obtain pre-curved glass tubes with different radii of curvature and diameters, which could allow the use of micro pre-curved glass tubes along with or in place of Nitinol. Using these micro pre-curved glass tubes could either improve existing robot performance or address new applications that require a more miniaturized robot backbone.

2.2 Glass CTR Deployment

The use of sub-millimeter pre-curved glass capillaries for CTR prototyping and their respective demonstrations of the deployment capabilities of the robot are discussed in this section. The rapid fabrication approach in our method enabled Caturo to be adaptable to various applications; this adaptability was made possible by imposing different tube specifications, as displayed in Table 1. The actuation unit for the robotized Caturo is described in Figure 1D, which uses open-loop control for the demonstrations.

3D conical-spiral free space deployment: Table 1 presents the tube specifications used to demonstrate this

s/n	Demonstration type	Inner tube				Outer tube			
		d_i [μm]	D_i [μm]	CT [μm]	R_i [mm]	d_e [μm]	D_e [μm]	CT [μm]	R_e [mm]
1	The Caturo (1B)	100	164	12	11.5	249	353	18	∞
2	3D conical-spiral (3A)	100	164	12	58.8	249	353	18	∞
3	Fluid suck & delivery (5B)	100	164	12	26.5	249	353	18	∞
4	Vitreoretinal deployment (5C)	20	90	12	8.9	249	353	18	∞
5	FKM (4A & 4B)	100	164	12	63	249	353	18	120
6	IKM (4C)	100	164	12	58.8	249	353	18	2x10^8
7	Instability analysis (4D)	100	164	12	42	249	353	18	92
		100	164	12	25	321	434	18	105
8	Needle constraint (3C)	100	164	12	54.4	321	434	18	∞
9	Helical precurved (3B)	100	164	12	H	321	434	18	∞
10	fibre optics precurved (5A)	0	125 F	61	40	321	434	18	∞

D_i: External diameter of inner tube including CT
D_e: External diameter of outer tube including CT
FKM: Forward kinematic model
d_i: Internal diameter of inner tube
d_e: Internal diameter of outer tube
IKM: Inverse kinematic model
R_i: Inner tube radius of curvature
R_e: Outer tube radius of curvature
F: Optical fibre
CT: Coating thickness
H: Helical shape

Table 1. The different demonstrations and Caturo tube specifications

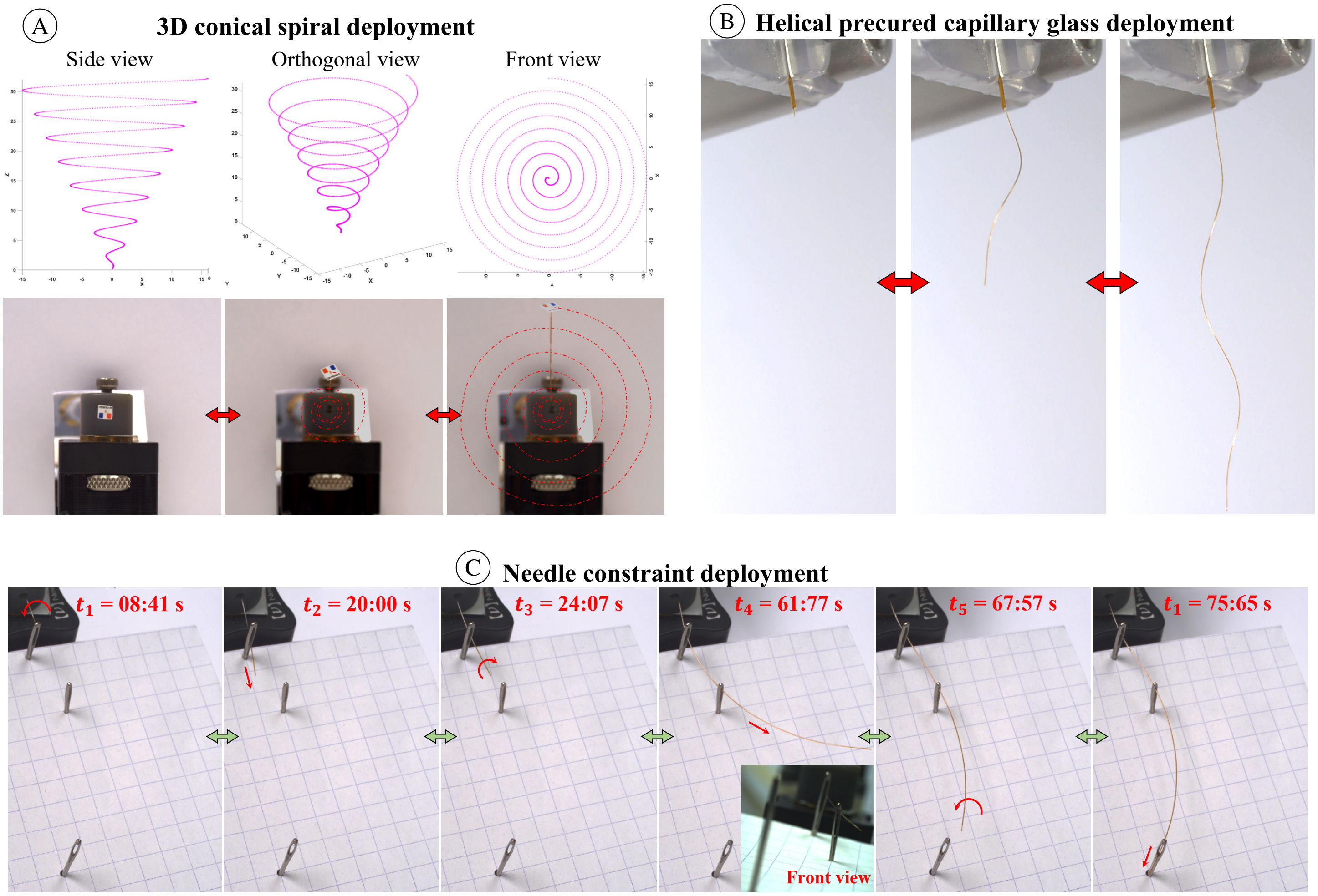

Figure 3. Demonstrations of deployment of the sub-millimeter pre-curved glass CTR. (A) A 3D conical-spiral trajectory free space deployment strategy; which has a 4 x 4 mm tip attachment for better visualization during the navigation; (B) Demonstration of a complex helical pre-curved glass tube free space deployment, showing the flexibility of the glass tube in forward and reverse movement; (C) The robot small scale size and its flexibility for a constraint path deployment maneuvering through a less than 1 mm orifice of three needles, using only one pre-curved tube with a 54.4mm radius of curvature.

free space deployment, as presented in Figure 3A, which is best represented by the Movie-S2 in the Supplementary section. The navigation path begins in the central region and extends in a conical-spiral pattern. The distinct nature of the 3D conical-spiral deployment is described by the simulation in Figure 3A, in which the side view shows a helical trajectory path; the orthogonal view shows a conical shape; and the front view shows a planar spiral navigation path. The experimental demonstration is presented in Figure 3A; for better visualization, a 4x4mm paper sheet with distinct colors was attached at the tip of the inner pre-curved tube during the deployment. The actuation unit prototype is displayed in Figure 1D. The conical-spiral path trajectory was achieved using the simultaneous rotation and translation of the inner pre-curved tube, which progressively expands in the workspace as it slides forward through a fixed outer straight tube and vice versa. This trajectory demonstrates the flexibility of the glass CTR under translational and rotational actuation.

Helical pre-curved CTR glass deployment: the novel fabrication approach of obtaining a pre-curved CTR glass tube was not limited to only the planar pre-curved shape. The approach was also applicable to other non-planar complex 3D shapes, such as a helix (Figure 2B). A circular helix mold design was used and parameterized as a function of the arc-length (s), which is obtained by: $[x(s), y(s), z(s)]^t = [rcos(s), rsin(s), bs]^t$. The radius (r) = 1mm, pitch = 2mm, $b = \frac{pitch}{2\pi}$ and the total arc-length = 32mm. The possibility of the free space deployment of a helical pre-curved glass CTR was demonstrated, as presented in Figure 3B. For this demonstration, the tube specification used is given in number 8 of Table 1, where a helical pre-curved inner tube slides through the straight outer tube. This presents a flexible helical Caturo and demonstrates its ability to straighten its 3D backbone shape during deployment without the glass fracturing (Movie-S3 in the Supplementary section). Similar to its planar pre-curved counterpart, irrespective of the complex shape of the pre-curved tube, the inherent flexible property is preserved. This best describes the concept of path-specific pre-curved tube prototype, obtained by adapting the complex desired path to the 3D printed mold.

Constraint deployment of CTR through needles: the glass Caturo was also used to demonstrate a constrained path deployment through the orifice of three stationed needles (each ∼1mm in width), as displayed in Figure 3C. It also involves a contact-aided deployment on path with a higher radius of curvature than the robot. The flexibility of glass pre-curved tubes here was exploited to allow us to maneuver the Caturo so that it could pass through three needle orifices to the distal point and safely navigate back again without the glass tube breaking during the navigation (Movie-S1 in supplementary). For this demonstration, off-the-shelf metallic needles were used. The needles were positioned at different cross-points on the paper (see Figure 3C). The specifications of the Caturo used for this demonstration are provided in Table 1; the actuation unit prototype is presented in Figure 1D. The robot was then programmed to automatically pass through each needle opening, which involved several translations and rotation maneuvering, to ensure the constrained path was maintained throughout the path deployment. This demonstration demonstrates the flexibility and capability of the Caturo in miniaturized task-specific applications that involve complex 3D navigation through a miniature-constrained path. To the best of our knowledge, this is the first robot made of glass to maneuver through a small orifice of this type and size. This broadens the potential of applications that involve accessing areas through a small-scale aperture, such as microsurgery.

2.3 Model Validation on Sub-millimetre Glass CTRs

For medical applications, CTR design is essential because it could help prevent permanent tube deformation and robot instability. When modeling CTR, there are inevitable trade-offs to be considered among accuracy, computational cost, and model complexity;[5] this also relates to the criteria. For the Caturo model validation, the piecewise constant curvature model was first used for the FKM and IKM due to its simplicity[2,48]. The stability analysis, which considers the additional effect of torsion, involved the use of Cosserat rod problem formulation.[49] In all the cases in which the classical elasticity theories were used, considering the robot's tube size, the effect of friction, extension, and shear were all neglected. The model validation and evaluation demonstrated are as follows:

Forward Kinematic Model (FKM): Inserting one curved tube into another curved tube causes their common axis to form a mutual resultant curvature at equilibrium. Due to the inherent compliance of continuum robots, elasticity is one essential factor for the kinematics. Their modeling and control are more complex than the traditional robots with rigid links. The pose of a traditional robot at any given point is fully defined in closed form by joint angle and link length. [50] The specifications of the Caturo used for this demonstration are provided in Table 1, and the actuation unit prototype is presented in Figure 1D. The torsionally rigid CTR model used here uses the simple arc geometry approach to the piecewise constant-curvature model; this approach was simulated and experimentally validated using the sub-millimeter glass CTR. The tube curvatures are positioned in the same plane in the aligned robot configuration in Figure 4A. The configuration was chosen because the planar robot shape is perpendicular to the camera view. To compare the robot's experimental backbone to that of the constant-curvature CTR model, MATLAB software was used to run the simulation and post-processing analysis. Comparing the experimental results to the model revealed a similarity along the robot's backbone, as presented in Figure 4A. There was a mean deviation of μ_x = 0.30mm, a standard deviation of σ_x = 0.17mm, and a percentage error of 0.83%. The same process was used for the case of anti-aligned robot configuration (where the two tube curvatures are aligned in opposite directions), as displayed in Figure 4B. The experimental robot's backbone closely matches the backbone of the model (see Figure 4B); comparing the two revealed a mean deviation of μ_x = 0.12mm, a standard deviation of σ_x = 0.07mm, and a percentage error of 0.47%. The results for both the aligned and anti-aligned cases indicate that the constant curvature CTR model can be adapted for the Caturo as well.

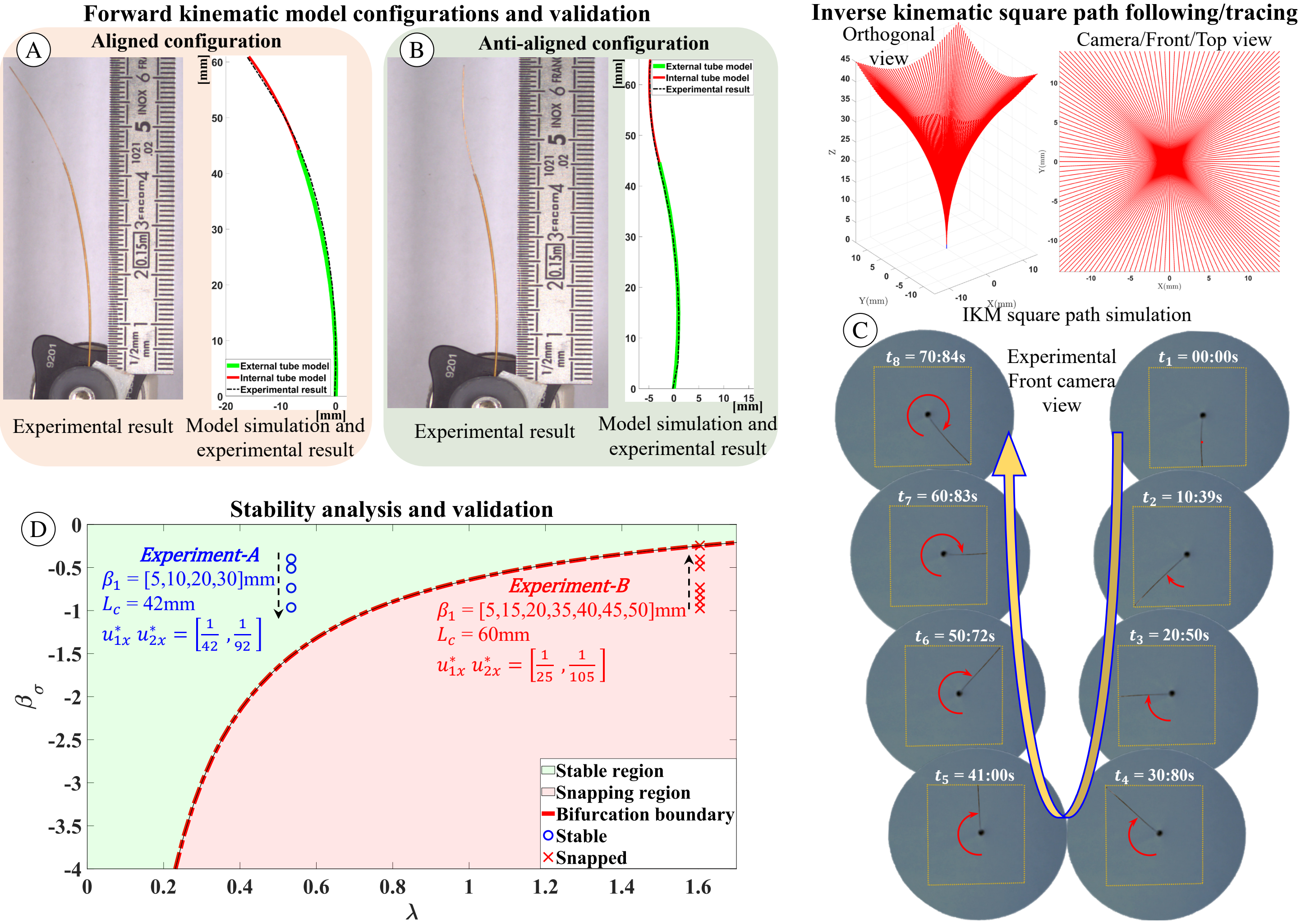

Figure 4. Sub-millimetre glass CTR model validation. **(A)** and **(B)** Experimental results, along with the CTR forward kinematic model validation and comparison, include the two different cases: aligned (where the two tubes are in the same direction) and anti-aligned (where the tubes are in the opposite direction). **(C)** View of the simulation results using a closed-form geometric approach to the inverse kinematic model. The approach is for a square path following system, which is characterized by two DoF and no end-effector position feedback control. **(D)** Stability analysis of micro-glass CTR under torsion, which is used to validate the effect of change in transmission length for two different cases, as displayed in *Experiment-A and Experiment-B* with a change in the curvature and active curve length of the tubes.

Inverse Kinematic Model (IKM) Based on Open Loop Control: The simple and fast closed-form geometric approach to IKM was used to control the end-effector pose in an open loop control scheme (see Figure S4 in Supplementary B). The IKM was used to generate the joint variables (q_i) for the discretized square path, as displayed in Figure 4C. For the experimental demonstration, an open loop IKM control base was implemented using a 2-DoF actuation unit, characterized by one translation and one rotation (refer to Figure 1D). The Caturo specification is provided in Table 1. The experiment was conducted by placing a camera fixed in the front (defined as the camera view in the simulation on Figure 4C) while the robot translates and rotates out of the plane. The square path tracing is a 2D projection on the front x, y plane, when viewing the distal end of the inner tube, for the IKM simulation and deployment. The experimental result for the square path presented in Figure 4C, and the video in Movie-S6 Supplementary, validates the possibility of actualizing path tracing. This validation is in line with the model simulation. The result obtained included the robot position accuracy with a root mean square error (RMSE) of 0.201mm ($RMSE = \sqrt{\frac{1}{n}\sum_i^n \|\hat{p}_i\, p_i\|^2} = \sqrt{\frac{1}{n}\sum_i^n (\hat{x}_i - x_i)^2 + (\hat{y}_i - y_i)^2}$, refer to Figure S5 in the Supplementary section). The linearity in the x-axis are $X_{down} = 4.9\%, X_{up} = 7.7\%$. The linearity in the y-axis are $Y_{right} = 3.7\%, Y_{left} = 10.1\%$. This demonstration proves that the IKM of CTR can be applied to the sub-millimeter glass CTR with a satisfactory result. It is especially noteworthy considering the fact that the robot was used in an open loop control without any visual servoing or closed loop feedback for intermediary error correction.

Stability analysis and validation: It is often desirable to use curvatures that are as high as possible when designing CTR. However, high curvatures could result in elastic instabilities. [11,49,51] The objective is to design robots that are guaranteed to remain elastically stable throughout the entire workspace. Instability has been one of the key challenges with CTRs being used in medical intervention. CTR instability due to torsion (known as snapping) is a sudden leap from one equilibrium configuration to another. This leap is accompanied by the release of accumulated torsional (twist) energy. This could lead to the damage of nearby fragile tissues or vital organs. This particular phenomenon has been linked to the robot's transmission length, the tube curvatures, length of the active overlaying tubes, friction, clearance between the tubes, and the ratio of tube torsion to bending stiffness. [1,3,52,53] There has been a greater focus on the first two aforementioned criteria in literature. To verify and evaluate the instability issues associated with the Caturo, two different experiments were carried out. Both experiments used different tube specifications, as displayed in Figure 4D and the tube specification provided in Table 1; the actuation unit is displayed in Figure 1D. The stability analysis was aimed at snap prediction to guarantee a snap-free robot. Snap prediction was facilitated using Equations presented in the Supplementary C section, based on the bifurcation and elastic stability theory [11,49,51,54] and the torsionally compliant model of CTR, which considers the effect of twisting. The experimental validation was then carried out to justify possible snapping due to torsion, in regard to the model prediction. The results indicate that in *Experiment-A*, for all the given values of transmission length, the robot operates within the stable region; this was the opposite in the case of *Experiment-B*, which was as predicted. Each test was observed for twice for clockwise and anti-clockwise rotations of the inner tube (see Movie-S7 in the Supplementary section). Based on the stability analysis result in Figure 4D, the higher the transmission length, the closer to the bifurcation boundary and vice versa. Irrespective of the transmission length, the tube curvature and the aligned active curve length of the tubes under torsion also influence instability, as seen from the comparison of *Experiment A and B*. According to this demonstration, the usual criteria and factors that work for Nitinol CTR are also applicable to the Caturo. When the bifurcation parameter λ exceeds the critical value λ_0, buckling will occur. [49] Therefore, comparing the glass and Nitinol tube material while considering the same geometrical parameters (e.g., tube curvatures and active curved length) leads to the bifurcation parameter $\lambda \propto 1 + \nu$, where ν is the material Poison ratio (refer to Supplementary C). Theoretically, this demonstrates that the relationship between the bifurcation parameter of glass λ_g and that of Nitinol λ_N tube is represented by $\lambda_g = 0.87\lambda_N$. This expression means that the glass tube material will have slightly less stability than the conventional Nitinol material under the same geometrical conditions.

2.4 Applications

The proposed application of CTR for medical intervention is quite vast, as discussed in the Introduction section. Although it could still be used for other applications aside from clinical intervention. In this section, the benefits of the miniature robot were explored. The intrinsic properties of glass for various demonstrations could lead to breakthroughs in medical applications.

Deployment of pre-curved optical fiber with laser transmission: Lasers are an important aspect of contemporary surgery. This is especially true for microsurgery, which often concerns procedures on small and fragile organs such as the eyes and vocal folds. [55–57] During medical interventions, lasers can cut tissue with precision due to their micron spot focusing capability and thermally seal blood vessels. Thermal sealing enables procedures with less blood loss. [55] The two robotic approaches for laser aiming are the free beam (this uses mirror deflection, which depends on the direct line of sight and is difficult to miniaturize for in vivo application) and the fiber-based approach (this uses optical fiber to remotely focus light on the surgical site). Passing optical fiber carrying laser is not the only route. CTR dexterity could be improved by using a pre-curved optical fiber as part of the robot backbone because the approach of bringing light to the surgical site is not limited by the direct line of sight (Movie-S4 in supplementary). To actualize this, a fusion splicing and joining of the pre-curved optical fiber with another long part that has the right connector at its end (Single Mode Fiber, Thorlabs) (see Supplementary E). The fusion ensured an effective connection to the laser source (Thorlabs-S1FC635). The outcome of the laser emission at the CTR tip is presented in Figure 5A. This demonstration of a pre-curved optic fiber Caturo opens a new prospect for light or thermal-controlled end-effectors or manipulators, as it would be beneficial for safe/precise robot-assisted

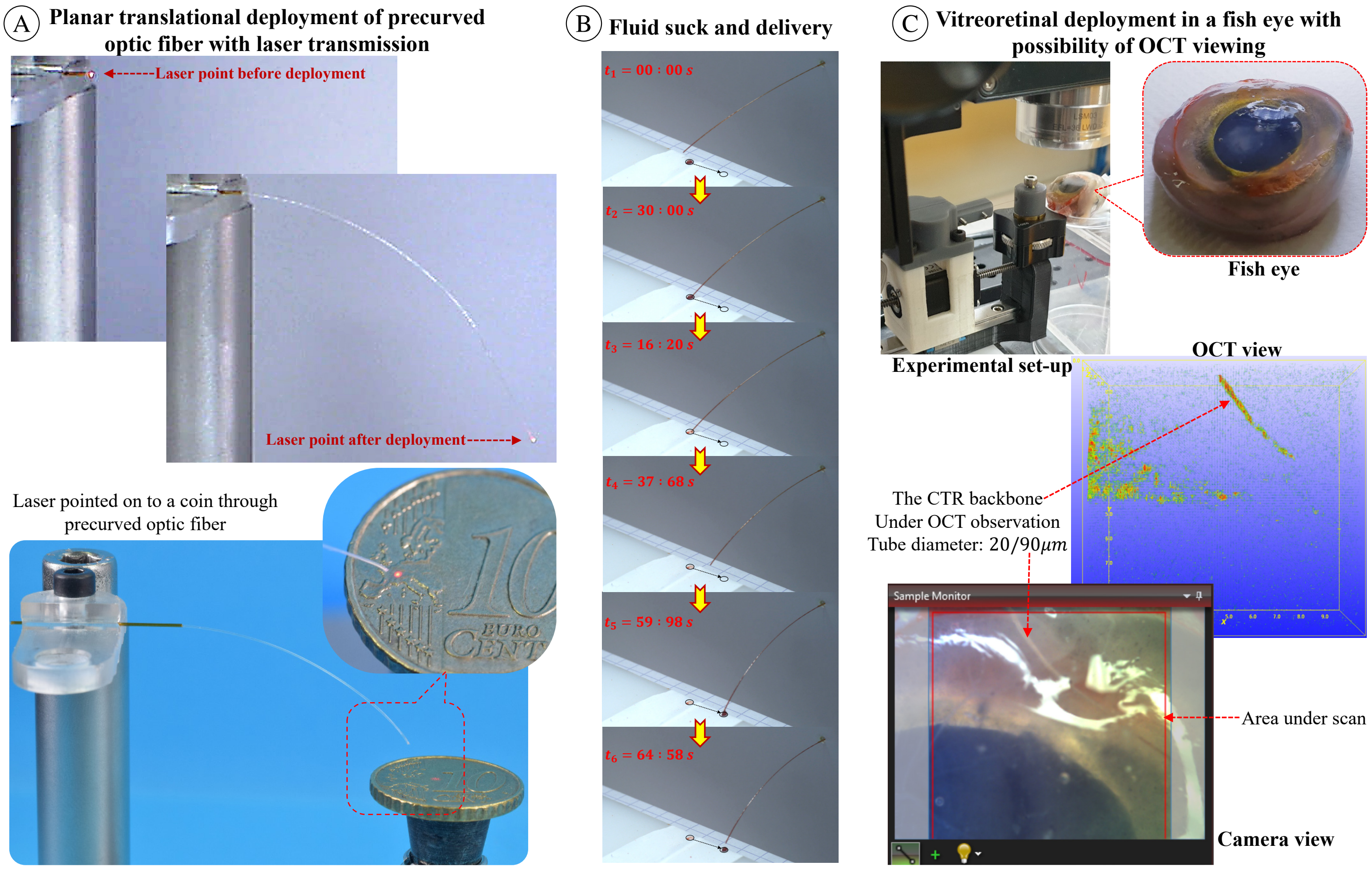

Figure 5. Different application of the micro-glass CTR. (A) The possibility of emitting laser through a pre-curved optical glass fiber to the end-effector tip, where the proximal end is connected to a laser source; (B) A two-in-one demonstration of the capability of the robot for either transferring a liquid sample or specimen from one point to another and its ability for drug delivery or sample collection; (C) Vitreoretinal deployment through an eye of a fish with an OCT viewing capability.

laser ablation.

Fluid suction and delivery: Compared to other members of the continuum robots family, the internal hollow cavity of a CTR is very beneficial. The internal hollow cavity can allow the passage of pressurized fluid (e.g., air and liquid) to the end-effector position for tip control or manipulation. The Caturo has the potential for drug delivery, as demonstrated in Figure 5B, in addition to its 3D path deployment capability. In the context of medical intervention, Figure 5B features a 2-in-1 demonstration (the ***ability for sample collection and biopsy***) and ***a drug delivery capability*** using the sub-millimeter glass CTR prototype. For this particular demonstration, a red ink sample (to mimic blood) was used. The distal end of the glass tube was connected to a manually operated pressurizing syringe (Figure 7). The robot was controlled to move to the sample collection location, which was followed by fluid suction operation and fluid delivery at the destination point, as displayed in Figure 5B. According to this demonstration, there is a possibility for pressurized fluid flow from the proximal point to the distal end through the inner tube cavity (Movie-S5 supplementary). The demonstration also revealed the ability to hold the fluid sample at the distal tip region with a controlled pressurized air of the syringe during sample transportation from the collection point to the delivery point. The Caturo tube specifications used for this demonstration are provided in Table 1. It had its internal tube glued to a long thin rubber pipe in order to connect to the syringe at the proximal end (Figure 7). Considering the miniature size of the robot and its ability to maneuver through 3D curves, this opens up the prospect for multiple minimally invasive interventions (e.g., quick biopsy and drug delivery) through a natural body orifice or through small incision access to the surgical site, such as vitreoretinal surgery.

Vitreoretinal deployment with the possibility of OCT viewing within a fish eye: Retinal microsurgery presents unique problems that are beyond the scope of current manual surgical technologies.[58] The use of robotic technologies in vitreoretinal surgery has been investigated to overcome the barriers of perception, tremor, and dexterity.[59,60] Moreover, the use of CTR for this application has been proposed in [19, 61–63]. The benefits of robotics in vitreoretinal surgery include the use of tremor filtration that can help overcome natural human limitations, improve dexterity, enable in vivo navigation without direct visibility, enable high precision/safety, and enable possible long-distance teleoperation procedures by a specialist. Although there is a challenge posed for this procedure: the eye is delicate and small with complex nerve interconnections. The characteristics of the eye make it challenging for MIS. Considering these factors, we operate in the sub-millimeter range, as presented in Figure 2B and Table 1. Vitreoretinal deployment operation is one of the target applications of this robot. Considering the internal composition of an eye (vitreous humor), CTR navigation as well as OCT visualization can be enabled. That is why we propose an ex vivo robot deployment, as presented in Figure 5C. The value of this robot (aside from its miniaturized size) is its high dexterity in small confined spaces while simultaneously avoiding sensitive areas during its 3D path movement inside the eye. The idea is to simply use the straight external tube, which is stiffer to puncture at the entrance point, while the large workspace inside the eye is explored with the combined use of the two tubes. In addition to their potential biomedical applications, the CTR tube materials are bio-compatible, which makes them potentially important assets in medicine and vitreoretinal surgery. In addition, preliminary results of the OCT-based position control of a CTR for an optical biopsy have already been proposed in [64].

3 DISCUSSION

Due to the high demand for robots in MIS, the valued specifications include smart capability, dexterity, and level of miniaturization.[65] It is important to consider the ability of CTR to reach its destination without relying on any external support or influence, but by mere tube actuation at its proximal end. Not only is the end-effector pose known, but the ability to estimate the entire robot backbone (Figure 4A), makes it ideal for in vivo anatomy deployment. The conformation of Caturo through validations (FKM, IKM, instability analysis) with the already existing model of CTR in the literature reveals information that could lead to further exploration of hard-to-reach areas.

CTR transmitting laser uses an optical fiber, which passes through the cavity of the inner tube.[66] This novel approach demonstrates that it is possible to obtain and use a pre-curved optic fiber as part of the robot's backbone (Figure 5). The constrained 3D path deployment, through the orifice (approximately 1 mm) of three positioned needles, highlights the maneuverability and flexibility of the robot by demonstrating its capability to follow the complex path in its entirety. Based on the demonstration of fluid suction and delivery operation of the robot in Figure 5B, there is a possibility of fluid or light-driven actuators/sensors for a functionalized end-effector integration. The demonstration presented in Figure 5B presents three functional capabilities associated with the Caturo: sample extraction ability (**Biopsy**), sample delivery capability (**Drug delivery**), and its ability to transport samples between points within an area of interest (**Manipulation**). The small size of a glass capillary can be used to mimic a butterfly proboscis. Such mimicking could potentially enable other CTR applications in the future outside of medicine, such as robot-assisted indoor pollination. Furthermore, the kinematic model analysis conducted did not take into account the effect of contact friction existing between the thin external polymer and the inner glass surface. Although friction, unlike stiffness, does not determine the shape of the robot, there is still space for further investigation in this area. There are currently a few models for this phenomenon (see [67, 68]), though they are much more complex and challenging to experimentally evaluate on a sub-millimeter scale.

3.1 Limitations and Challenges

The spring-back effect is a challenge in the fabrication of CTR tubes using thermal treatment approaches. This effect was also observed in the case of conventional Nitinol CTR tubes (with the traditional air furnace-based shape setting and the electric joule heating technique)[69]. Concerning the glass tube diameter, the diameter increased as the obtainable radius of curvature increased, as the micro-glass tube became stiffer to bend and less effective. This approach is quite suitable for sub-millimeter diameter glass tubes in the range of $< 500\mu$m. As a result, it can be complementary with an approach involving Nitinol or even hybridized to take advantage of both methods. Since the pre-curved glass tube is fixed in bending by the heat-shrink polymer, any defect in the polymer will affect the resultant tube shape. This influence on the tube shape leads to the possibility of pre-curved edges degrading over time as they slide against the sharp tip of the outer tube. For a higher curvature, this demands a thicker heat-shrink polymer that directly increases the external diameter of the pre-curved tube, which makes it challenging to slide into another during deployment. It is possible for there to be more than two glass CTR tubes, as demonstrated in 1C. However, one needs to take into account the permissible clearance that will guarantee smooth sliding between each concentric tube. For this purpose, we are limited to the commercially available dimensions (Polymicro Technologies). This study was also conducted under the constraint of using tubes $< 500\mu$m in diameter. The tube diameter depends on the commercially available dimensions, but the smallest tube size in this experiment is the **tube-1**$= 90 : 20$ μm, with an achievable radius of curvature of ∼5mm (Refer to Figure 7B and Figure S1 in the Supplementary section).

3.2 Integration of micro end-effectors

Functionalizing CTR with an effector is vital for task-specific applications. CTR end-effectors are often wire-driven. In the literature, the smallest diameter size is 1 mm [70], which would be unsuitable for the sub-millimeter glass CTR. Integrating an end-effector into the sub-millimeter glass CTR tip is challenging due to the difficulties associated with microfabrication. Although the possibility of actualizing this will be beneficial for the use of small-scale and application-specific tasks in clinical interventions. The two major considerations for micron-size end-effector integration are typically the use of light-driven and pressurized fluid through the innermost tube aperture. Glass capillaries could guide light to actuate a thermal micro-gripper [71] or an optical fiber tip self-regulated photo-mechanical actuator system with a contactless sensing probe. [72] Several microfluidic principles, such as micro-pistons, can be exploited for tip actuation as well. [73] Some of the possible pneumatic or hydraulic end-effectors that could be integrated into the glass CTR tip include a 3D 100μm compliant end-effector with an integrated force sensor [74], a 150μm capillary tip microgripper [75], and a 0.15mm^2 micro piston actuator. [76]

Nitinol is currently the predominant material used for CTR design and prototyping, but there are some drawbacks regarding the level of miniaturization and on-site patient-specific fabrication. This challenge can be alleviated by using micro-glass tubes as an alternative. Micro-glass tubes have the benefits of the obtainable tube properties (e.g., lowest radius of curvature, three times smaller compared to that of Nitinol in the literature of 15 mm [33]) and sub-millimeter pre-curved tube sizes with the smallest obtainable external diameter (glass has a diameter of 0.09 mm, while the CTR Nitinol tube in the literature has a diameter of 0.41 mm. [19] However, one can obtain a straight Nitinol tube with an external diameter of 0.25 mm online (Johnson Matthey). In addition, there is also the possibility for on-site fabrication of complex shapes or patient-specific pre-curved tubes due to the 3D print mold requirement. This fabrication method is less time-consuming, has a lower temperature, and is less expensive compared to that of Nitinol tubes.

4 Methods/Experimental Section

Tube shaping: It is possible to use only heat-shrink plastic tubing to obtain a pre-curved CTR tube, as demonstrated in [77, 78]. The process involved using a pre-curved wire as a mold and a heat gun for thermal treatment. The resultant tube had a diameter range on the millimeter scale after shrinkage and a large radius change deformation. Thus, it was only used for the inner CTR tube. To overcome these challenges, we adopted an approach that involves the use of two materials: 1) a thin heat-shrink polymer to enforce shape setting and 2) flexible glass capillaries as the robot's active backbone. The step-by-step heat treatment fabrication procedure to obtain pre-curved glass tubes for CTR using a thin heat-shrink polymer (from Nordson Medical) is described in Figure 6A. The design of every pre-curved tube begins by understanding the correct tube specifications (e.g., the inner and outer tube diameters, the tube length, and the material used, which affects the fabrication approach to be adopted). In this novel approach, commercially available straight micro-glass tubes (Molex glass capillary) and commercially available thin heat-shrink polymer tubing were used to obtain pre-curved tubes (Figure 2B) using a heat treatment at about 300°C in a furnace. The fabrication approach was characterized and validated for two heat treatment du-

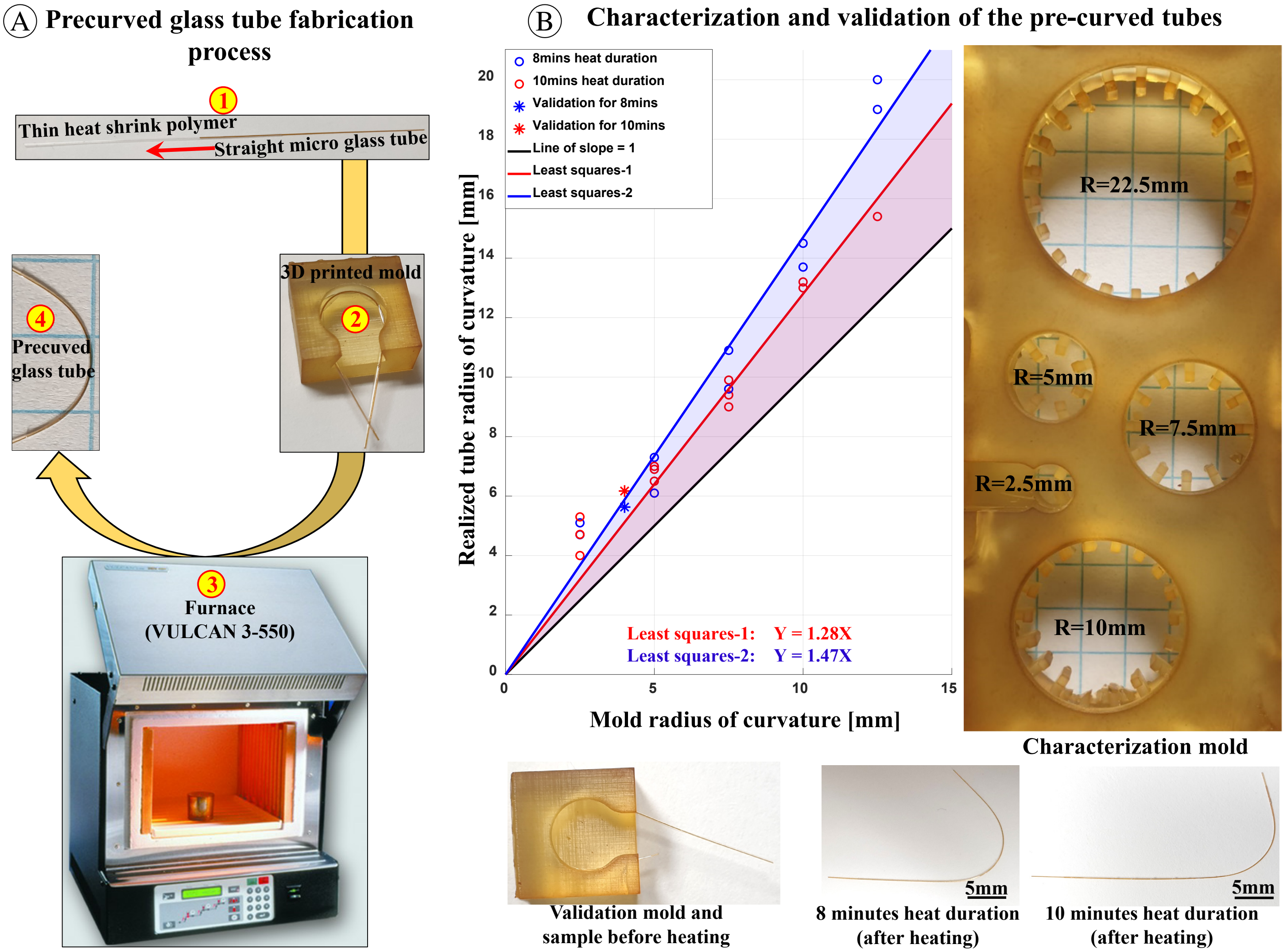

Figure 6. The pre-curved tube fabrication process. **(A)** The fabrication procedure for obtaining a pre-curved glass tube has steps that include: 1) inserting the glass capillary into the thin heat-shrink polymer tubing; 2) constraining it to the desired 3D printed mold shape; 3) applying thermal treatment in the furnace for a short period; and 4) obtaining the pre-curved micro-glass tube. **(B)** The characterization and validation of the novel fabrication approach were conducted for two different heat durations. The circle points are the various results. The lines are the least square algorithm. The radius of curvature in Y to the mold radius of curvature in X was validated, as demonstrated by the star points on the plot.

rations (eight and ten minutes) by using five different mold curvatures, as shown in Figure 2B. The specification of the heat-shrink polymer tubing used has a thickness of 6µm with an external diameter of 254µm. The glass capillary has an inner diameter of 20µm and an external diameter of 90µm. In order to ascertain the spring-back effect (which denotes the measure of deviation from the desired curvature), the outcome of the characterization test as a result of heat treatment duration for the different mold radii of curvature was obtained. This outcome is presented in Figure 6B. The result obtained shows a level of linearity that was evaluated using the least square algorithm. The result of this evaluation is the straight line plot and equation displayed in Figure 6B, which relates the realized radius of curvature in $y-axis$ to the mold radius of curvature in $x-axis$. A 10-minute heat duration (represented in red) with almost a unit slope means that the realized radius of curvature due to the spring-back effect will fall within 1.28 mm of the mold radius of curvature and likewise for the 8-minute heat duration. This relationship was further validated, as represented by the star points in Figure 6B, for the two temperature durations. In the experimental validation, a new 3D-printed mold with a $4mm$ radius of curvature was fabricated, and the realized tube radius of curvature was evaluated for the two temperature heating durations. The result of the validation (indicated by the star points on the characterization plot) shows the linearity, which was obtained while accounting for the two heat durations and how close they are to the least square line. The black line with a slope of 1 in Figure 6B represents the ideal scenario, where the realized tube radius of curvature is equal to the mold radius of curvature. This is not obtainable due to the spring-back effect, which can be represented as the colored boundary using the least square line plots. Furthermore, the effect of creep was investigated in order to analyze the relaxation of the pre-curved tube over several days. This effect was just noticeable between the first and the second day after fabrication, with an acceptable relaxation of around 10%. The relaxation became very minimal later in the day. Generally, the results obtained with the specified heat shrink and the glass tube were satisfactory. The result can also be extended to other different dimensions or specifications of interest. The advantage of this method compared to the Nitinol-based approach is that it does not require high temperatures and a long heat duration. These two factors permit the use of the 3D printed mold (Formlabs stereolithography printer using FLHTAM02 material). They allow the convenient fabrication of complex shapes. Even a patient-specific pattern can be imposed.

Numerical simulation and evaluations: For the numerical modeling and data processing simulation analysis, the MATLAB software was used. The analysis includes the arc geometry approach to piecewise constant-curvature FKM (Figure 4A $\&$ 4B), the closed-form geometric approach to IKM (Figure 4C), and the stability evaluation of Figure 4D. In addition, the software was used for data processing of the fabrication process characterization (Figure 6B) and other analyses in the Supplementary section.

For the FKM, the use of piecewise constant-curvature approximation simplified the kinematic modeling of continuum robots using two mapping decompositions. It was simplified by treating it as a discretized link section made of arc parameters. The CTR kinematics is usually mapped between: **the actuator space** (the joint variable consisting of the translation and rotation of each individual tube of the robot *(q)*), **the configuration space** (which are the robot backbone parameters *(κ, ϕ, l)*, and **the task space** (the tip pose due to the resultant shape of the robot backbone *(x)*), presented in Figure S3 in the Supplementary section. This constant curvature model was considered, and the dimensions and properties of each tube were imposed along with the joint variables of the robot. In addition, the arc geometry transformation approach was used to derive the pose of the robots from base to tip. Image post-processing was completed by extracting the robot backbone and re-scaling, after which polynomial curve fitting was used to normalize points on the plot curve for simpler evaluation. The comparison is in Figure 4A.

The bending stiffness analysis: To analyze the effect of the heat shrink on the micro-glass tube, bending stiffness was tested using three points method (Refer to Supplementary D). The bending stiffness was analyzed and plotted (refer to Figure S6 and Table S2) for three different dimensions of capillary glass tubes. The effect in cases with and without the heat-shrink polymer was also considered. The experimental result, comparing the bending stiffness ratio between the tubes without heat shrink and those with heat shrink, yields 1:1.61, 1:1.18, and 1:1.14 for three different glass tubes with the dimensions of $T_1 = 90/20$, $T_2 = 165/100$, and $T_3 = 356/249$ respectively. This result means that the effect of bending stiffness with regard to heat shrink is more significant with the smallest diameter and decreases as the tube diameter increases. The result indicates that this approach best fits small glass diameters ($< 500\mu$m). Additionally, when considering the same tube material, the bending stiffness is proportional to the moment area of inertia. The moment area of inertia is a function of the internal and external tube diameters, and its ratio between T_2 and T_1 is 1:6. The ratio for T_3 and T_1 is 1:122; this corresponds to the experimental result that shows an increment in bending stiffness as the tube dimension increases. It also explains why we assume dominance stiffness pair for the kinematic modeling. Young's modulus is derived from the experimentation. However, the micro-glass tubes (25-48GPa) tend to differ from the standard values of fused silica, which have a value of 72.9 GPa. [79]

CTR glass tube assembly: The arrangement and assembly of the sub-millimeter CTR glass tubes are the same as those of conventional CTRs (Figure 1A). The outer tube is usually straight with less curvature and is stiffer in conventional CTRs. Tube-1, tube-2, and tube-3 have external diameter to inner diameter of 90:20, 165:100, and 356:249, respectively. Therefore, there is a bending stiffness ratio between the possible combinations of tube-1 and tube-3 of 122:1. The ratio for tube-2 and tube-3 is 19:1. Considering the high stiffness ratios, the dominance stiffness approach illustrated in Figure 1A was used. In this approach, each successive inner tube conforms to the shape of the stiffer outer tube before deployment and then takes its original shape as it extends out during deployment. The schematic diagram and CAD design of the actuation unit for each demonstration is presented in

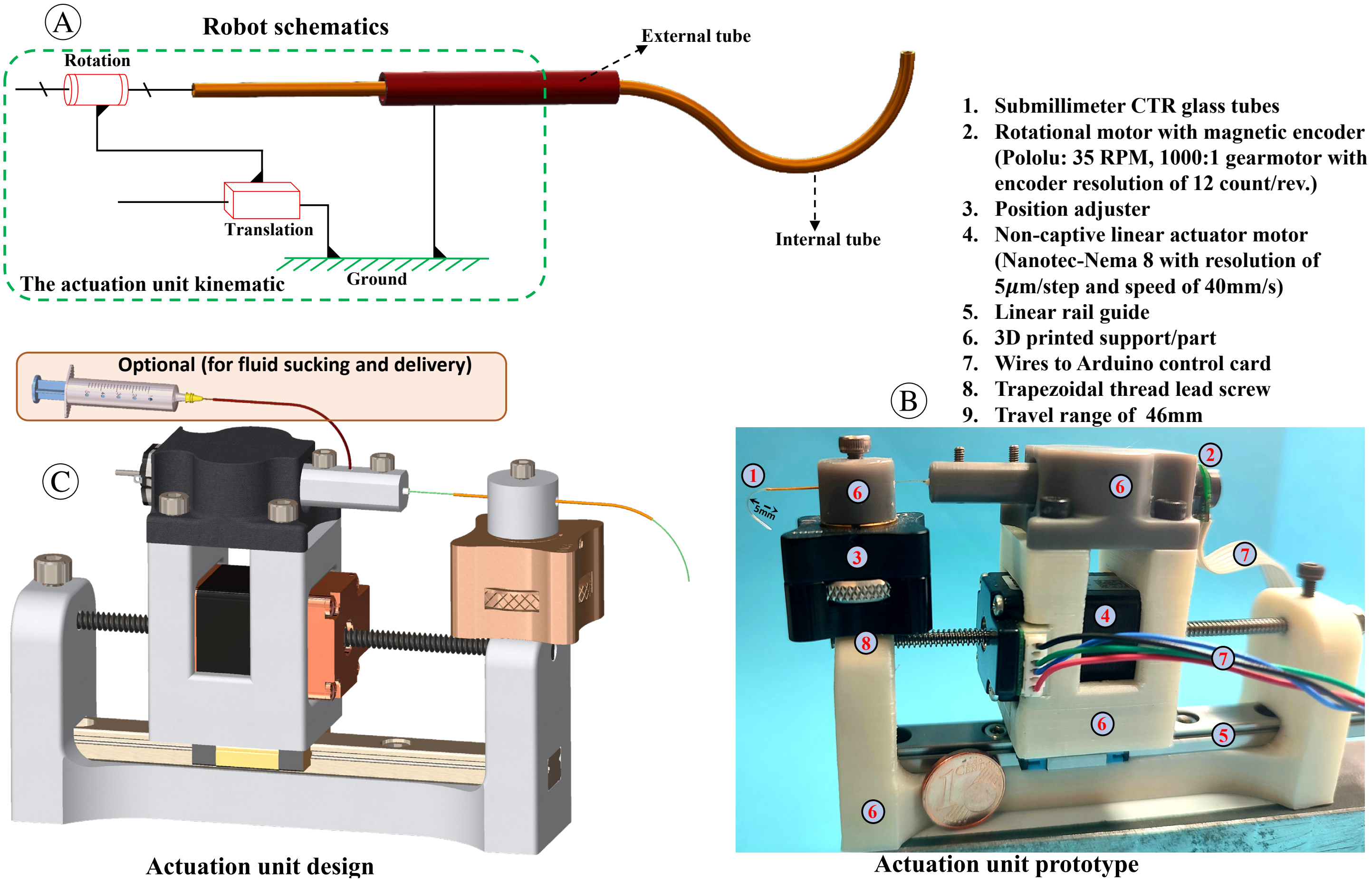

Figure 7. The Caturo CTR actuation unit design, showing the description of the CTR tube arrangement procedure and its deployment principle, **(A)** The design of the robot consisting of the schematic and **(B)** the CAD and **(C)** the realised prototype with the vital parts identified. The robot has two sections: the tube and the actuation unit.

Figure 7. The outer tube is always fixed in position, while the inner tube is characterized with two DoF.

CTR actuation unit: The schematic of the Caturo actuation unit architecture is presented in Figure 7A. The schematic includes two DoF (translation and rotation) that actuate the inner tube while the outer tube is fixed to the ground. The majority of the actuation unit design parts are 3D printed (Figure 7B) for fast prototyping and to benefit from lightweight material. The actuation unit design has optional features for inner tube connectivity for either light or hydraulic integration for end-effector manipulation. One example is the fluid suction and delivery operation using a syringe (Figure 7C). The designed prototype is small (10 cm × 2.5 cm × 5.4 cm) compared to many conventional CTR actuation unit prototypes in the literature. The components of the actuation unit design are identified in Figure 7B. The non-captive linear motor, which is mounted on the rail guide for smoother movement, is used for the transitional actuation. The miniature dual-shift gear motor with an encoder is used to actuate the rotation of the inner tube. The control was programmed and executed by the Uno Arduino board, which has a motor shield connected for efficient motor operation. The robot deployment was also controlled with a miniaturized joystick (SKU:BTN-026) that was connected to the Arduino for demonstration, similar to the 3D conical-spiral deployment.

5 Conclusion

There was a gradual shift from traditional open surgery to MIS due to its benefits. In addition, there is demand for further miniaturization, which could lead to possible deployment through sub-millimeter incision access to the surgical site or natural body orifice. This technology is particularly relevant in neurosurgery and microsurgery. All these advancements have led to the development of more innovative medical MIS tools and smarter devices. For this reason, we propose a sub-millimeter glass CTR called Caturo. Caturo is flexible, dexterous, and miniaturized, with the ability to pass through a 3D path to the site of interest. The novel approach of obtaining various pre-curved tube shapes in glass was achieved through thermal treatment with a thin heat-shrink polymer. The sub-millimeter diameter range (all tubes $< 500\mu$m) is what made it possible to obtain a stringent and unprecedented radius of curvature for the tube as low as 5 mm. Compared to Nitinol, this one has potential for on-site fabrication and patient-specific procedures. It is low-cost, fast, and does not demand a very high temperature or time-consuming heating process, unlike Nitinol. In addition, PET/glass has the benefit of reduced friction compared to conventional Nitinol/Nitinol, which is another very important aspect. The spring-back effect associated with this approach was also characterized. By adapting the existing CTR model to the validation of the Caturo, we were able to validate the forward kinematics model, the inverse kinematics model, and the stability analysis of the robot. Finally, various demonstrations were carried out to present the micromanipulation capability of the robot.

Supporting Information

Supporting Information is available from the Wiley Online Library or from the author.

Acknowledgements

We thank Pierre Roux for assisting in the prototyping of the robot and Michaël Gauthier for his valuable suggestions about the manuscript. This work was supported by the Région de Bourgogne-Franche-Comté, the ANR project μRoCS (ANR-17-CE19-0005), the ROBOTEX network (TIRREX ANR-21-ESRE-0015), and by EUR EIPHI program (ANR-17-EURE-0002).

Conflict of Interest

The authors declare that they have no competing conflicts of interest.

Data Availability Statement

The data that support the findings of this study are available from the corresponding author upon reasonable request.

References

[1] R. J. Webster, J. M. Romano, N. J. Cowan, *IEEE Transactions on Robotics* **2009**, *25*, 1 67.

[2] I. Robert J. Webster, B. A. Jones, *The International Journal of Robotics Research* **2010**, *29*, 13 1661.

[3] P. E. Dupont, J. Lock, B. Itkowitz, E. Butler, *IEEE Transactions on Robotics* **2009**, *26*, 2 209.

[4] J. Furusho, T. Ono, R. Murai, T. Fujimoto, Y. Chiba, H. Horio, In *IEEE International Conference Mechatronics and Automation, 2005*, volume 1. **2005** 410–415 Vol. 1.

[5] J. Burgner-Kahrs, D. C. Rucker, H. Choset, *IEEE Transactions on Robotics* **2015**, *31*, 6 1261.

[6] H. Alfalahi, F. Renda, C. Stefanini, *IEEE Transactions on Medical Robotics and Bionics* **2020**, *2*, 3 410.

[7] E. Amanov, T.-D. Nguyen, J. Burgner-Kahrs, In *Medical Imaging*, volume 9415. **2015** 94151.

[8] T. K. Morimoto, A. M. Okamura, *IEEE Transactions on Robotics* **2016**, *32*, 6 1419.

[9] M. T. Chikhaoui, K. Rabenorosoa, N. Andreff, *Mechanism and Machine Theory* **2016**, *104* 234.

[10] H. B. Gilbert, J. Neimat, R. J. Webster, *IEEE Transactions on Robotics* **2015**, *31*, 2 246.

[11] Q. Peyron, K. Rabenorosoa, N. Andreff, P. Renaud, *Mechanism and Machine Theory* **2019**, *132* 176.

[12] T. K. Rafael Ribeiro Silveira, Christian Louter, In *Challenging Glass 6 - Conference on Architectural and Structural Applications of Glass, TU Delft, Netherlands*, ISBN 978-94-6366-044-0, **2016** 135–148.

[13] S. M. Garner, X. Li, m.-H. Huang, *Introduction to Flexible Glass Substrates*, chapter 1, 1–33, John Wiley & Sons, Ltd, ISBN 9781118946404, **2017**.

[14] M. Farooq, B. Xu, S. Y. Ko, *BioMedical Engineering OnLine* **2019**, *18*.

[15] A. V. Kudryavtsev, M. T. Chikhaoui, A. Liadov, P. Rougeot, F. Spindler, K. Rabenorosoa, J. Burgner-Kahrs, B. Tamadazte, N. Andreff, *IEEE Robotics and Automation Letters* **2018**, *3*, 3 2315.

[16] G. Dwyer, F. Chadebecq, M. T. Amo, C. Bergeles, E. Maneas, V. Pawar, E. V. Poorten, J. Deprest, S. Ourselin, P. De Coppi, T. Vercauteren, D. Stoyanov, *IEEE Robotics and Automation Letters* **2017**, *2*, 3 1656.

[17] Y. Lu, C. Zhang, S. Song, M. Q.-H. Meng, In *IEEE International Conference on Information and Automation (ICIA)*. **2017** 299–304.

[18] H. B. Gilbert, R. J. Hendrick, R. J. Webster, *IEEE Transactions on Robotics* **2016**, *32*, 1 20.

[19] F. Lin, C. Bergeles, G. Yang, In *37th Annual International Conference of the IEEE Engineering in Medicine and Biology Society (EMBC)*. **2015** 5280–5284.

[20] D. Y. Lee, J. Kim, J. S. Kim, C. Baek, G. Noh, D. N. Kim, K. Kim, S. Kang, K. J. Cho, *IEEE Transactions on Robotics* **2015**, *31*, 6 1311.

[21] P. J. Swaney, H. B. Gilbert, R. J. Hendrick, O. Commichau, R. Alterovitz, R. J. {Webster III}, *Hamlyn Symposium on Medical Robotics* **2015**, 37–38.

[22] P. J. Swaney, A. W. Mahoney, A. A. Remirez, E. Lamers, B. I. Hartley, R. H. Feins, R. Alterovitz, R. J. Webster, *IEEE International Conference on Robotics and Automation (ICRA)* **2015**, 5378–5383.

[23] J.-S. Kim, D.-Y. Lee, K. Kim, S. Kang, K.-J. Cho, In *IEEE International Conference on Robotics and Automation (ICRA)*. **2014** 5871–5876.

[24] J. Burgner-Kahrs, H. B. Gilbert, J. Granna, P. J. Swaney, R. J. Webster, In *IEEE/RSJ International Conference on Intelligent Robots and Systems*. **2014** 1269–1275.

[25] H. Azimian, P. Francis, T. Looi, J. Drake, In *IEEE/RSJ International Conference on Intelligent Robots and Systems*. **2014** 2030–2035.

[26] D. B. Comber, E. J. Barth, R. J. Webster III, J. S. Neimat, In *Conference: The Hamlyn Symposium on Medical Robotics*. **2013** 112–113.

[27] J. Burgner, P. J. Swaney, R. A. Lathrop, K. D. Weaver, R. J. Webster, *in IEEE Transactions on Biomedical Engineering* **2013**, *60*, 9 2567.

[28] C. M. Graves, A. Slocum, R. Gupta, C. J. Walsh, In *IEEE International Conference on Robotics and Automation*. **2012** 709–714.

[29] A. H. Gosline, N. V. Vasilyev, E. J. Butler, C. Folk, A. Cohen, R. Chen, N. Lang, P. J. Del Nido, P. E. Dupont, *International Journal of Robotics Research* **2012**, *31*, 9 1081.

[30] D. C. Rucker, Doctoral dissertation, Vanderbilt University, **2011**.

[31] R. A. Lathrop, D. C. Rucker, R. J. Webster, In *IEEE International Conference on Robotics and Automation*. **2010** 5601–5606.

[32] D. C. Rucker, R. J. Webster III, G. S. Chirikjian, N. J. Cowan, *The International Journal of Robotics Research* **2010**, *29*, 10 1263.

[33] P. Sears, P. Dupont, In *IEEE/RSJ International Conference on Intelligent Robots and Systems*. **2006** 2850–2856.

[34] M. F. Rox, D. S. Ropella, R. Hendrick, E. Blum, R. P. Naftel, H. C. Bow, S. D. Herrell, K. D. Weaver, L. B. Chambless, R. J. Webster III, *IEEE/ASME Transactions on Mechatronics* **2020**.

[35] J. Burgner, D. C. Rucker, H. B. Gilbert, P. J. Swaney, P. T. Russell, K. D. Weaver, R. J. Webster, *IEEE/ASME Transactions on Mechatronics* **2014**, *19*, 3 996.

[36] T. Morimoto, J. Cerrolaza, M. Hsieh, K. Cleary, A. Okamura, M. G. Linguraru, In *Annual International Conference of the IEEE Engineering in Medicine and Biology Society*, volume 2017. **2017** 165–168.

[37] T. K. Morimoto, E. W. Hawkes, A. M. Okamura, *in IEEE Robotics and Automation Letters* **2017**, *2*, 3 1579.

[38] R. J. Webster, A. M. Okamura, N. J. Cowan, In *2006 IEEE/RSJ International Conference on Intelligent Robots and Systems*. **2006** 2857–2863.

[39] E. Cuellar, D. Roberts, L. Middleman, *Fiber and Integrated Optics* **1987**, *6*, 3 203.

[40] Y. Bellouard, *Opt. Mater. Express* **2011**, *1*, 5 816.

[41] M. Tomozawa, *Annual Review of Materials Science* **1996**, *26*, 1 43.

[42] L. Wondraczek, E. Bouchbinder, A. Ehrlicher, J. Mauro, R. Sajzew, M. Smedskjaer, *Advanced Materials* **2022**, *34* 2109029.

[43] L. M. Barker, R. E. Hollenbach, *Journal of Applied Physics* **1970**, *41*, 10 4208.

[44] M. J. Matthewson, In D. K. Paul, editor, *Fiber Optics Reliability and Testing: A Critical Review*, volume 10272. International Society for Optics and Photonics, SPIE, **1993** 34 – 61.

[45] B. Luethi, R. Reber, J. Mayer, E. Wintermantel, J. Janczak-Rusch, L. Rohr, *Composites Part A: Applied Science and Manufacturing* **1998**, *29*, 12 1553.

[46] J. H. Kim, T. J. Kang, W. Yu, *Journal of biomechanics* **2008**, *41 15* 3202.

[47] W. Xu, F. Zhou, C. Ouyang, W. Ye, M. Yao, B. Xu, *Journal of biomedical materials research. Part A* **2010**, *92,1* 1.

[48] S. Neppalli, M. A. Csencsits, B. A. Jones, I. D. Walker, *Advanced Robotics* **2009**, *23*, 15 2077.

[49] H. B. Gilbert, R. J. Hendrick, R. J. Webster III, *IEEE Transactions on Robotics* **2015**, *32*, 1 20.

[50] P. Dupont, N. Simaan, H. Choset, C. Rucker, *Proceedings of the IEEE* **2022**, 1–24.

[51] R. J. Hendrick, H. B. Gilbert, R. J. Webster, In *2015 IEEE International Conference on Robotics and Automation (ICRA)*. **2015** 2256–2263.

[52] R. J. Webster, J. M. Romano, N. J. Cowan, In *IEEE International Conference on Robotics and Automation*. **2008** 3888–3895.

[53] C. Girerd, K. Rabenorosoa, P. Rougeot, P. Renaud, In *2017 IEEE/RSJ International Conference on Intelligent Robots and Systems (IROS)*. **2017** 5661–5887.

[54] J. Ha, F. C. Park, P. E. Dupont, In *2014 IEEE/RSJ International Conference on Intelligent Robots and Systems*. **2014** 864–870.

[55] L. Fichera, *Science Robotics* **2021**, *6*, 50 eabf1523.

[56] L. S. Mattos, G. Dagnino, G. Becattini, M. Dellepiane, D. G. Caldwell, In *2011 IEEE/RSJ International Conference on Intelligent Robots and Systems*. **2011** 1359–1365.

[57] L. S. Mattos, A. Acemoglu, A. Geraldes, A. Laborai, A. Schoob, B. Tamadazte, B. Davies, B. Wacogne, C. Pieralli, C. Barbalata, D. G. Caldwell, D. Kundrat, D. Pardo, E. Grant, F. Mora, G. Barresi, G. Peretti, J. Ortiz, K. Rabenorosoa, L. Tavernier, L. Pazart, L. Fichera, L. Guastini, L. A. Kahrs, M. Rakotondrabe, N. Andreff, N. Deshpande, O. Gaiffe, R. Renevier, S. Moccia, S. Lescano, T. Ortmaier, V. Penza, *Frontiers in Robotics and AI* **2021**, *8*.

[58] P. E. Dupont, B. J. Nelson, M. Goldfarb, B. Hannaford, A. Menciassi, M. K. O'Malley, N. Simaan, P. Valdastri, G.-Z. Yang, *Science Robotics* **2021**, *6*, 60 eabi8017.

[59] E. Z. Ahronovich, N. Simaan, K. M. Joos, *Advances in Therapy* **2021**, *38* 2114 .

[60] M. Zhou, Q. Yu, K. Huang, S. Mahov, A. Eslami, M. Maier, C. P. Lohmann, N. Navab, D. Zapp, A. Knoll, M. A. Nasseri, *IEEE Transactions on Industrial Electronics* **2020**, *67*, 8 6617.

[61] L. Wu, B. L.-W. Tan, H. Ren, In *2015 IEEE International Conference on Robotics and Biomimetics (ROBIO)*. **2015** 368–373.

[62] M. Zhou, X. Hao, A. Eslami, K. Huang, C. Cai, C. Lohmann, N. Navab, A. Knoll, M. A. Nasseri, C. Xia, *IEEE Access* **2019**, *PP* 1.

[63] W. Wei, R. E. Goldman, H. F. Fine, S. Chang, N. Simaan, *IEEE Transactions on Robotics* **2009**, *25*, 1 147.

[64] Y. Baran, K. Rabenorosoa, G. J. Laurent, P. Rougeot, N. Andreff, B. Tamadazte, In *2017 IEEE/RSJ International Conference on Intelligent Robots and Systems (IROS)*. **2017** 3000–3005.

[65] G.-Z. Yang, J. Bellingham, P. E. Dupont, P. Fischer, L. Floridi, R. Full, N. Jacobstein, V. Kumar, M. McNutt, R. Merrifield, et al., *Science robotics* **2018**, *3*, 14 7650.

[66] D. V. A. Nguyen, C. Girerd, Q. Boyer, P. Rougeot, O. Lehmann, L. Tavernier, J. Szewczyk, K. Rabenorosoa, *IEEE Robotics and Automation Letters* **2022**, *7*, 1 462.

[67] J. Lock, P. E. Dupont, In *2011 IEEE International Conference on Robotics and Automation*. **2011** 1139–1146.

[68] J. Ha, G. Fagogenis, P. E. Dupont, *IEEE Transactions on Robotics* **2019**, *35*, 2 353.

[69] H. B. Gilbert, R. J. Webster, *IEEE Robotics and Automation Letters* **2016**, *1*, 1 98.

[70] P. E. Dupont, J. Lock, E. Butler, In *2009 IEEE International Conference on Robotics and Automation*. **2009** 3851–3858.

[71] A. Benouhiba, L. Wurtz, J.-Y. Rauch, J. Agnus, K. Rabenorosoa, c. clévy, *Advanced Materials* **2021**, *33*.

[72] O. Wani, H. Zeng, A. Priimagi, *Nature Communications* **2017**, *8* 15546.

[73] M. D. Volder, D. Reynaerts, *Journal of Micromechanics and Microengineering* **2010**, *20*, 4 043001.

[74] M. Power, A. Thompson, S. Anastasova, G.-Z. Yang, *Small* **2018**, *14* 1703964.

[75] A. Barbot, M. Power, F. Seichepine, G.-Z. Yang, *Science Advances* **2020**, *6*, 22 5660.

[76] M. De Volder, F. Ceyssens, D. Reynaerts, R. Puers, *Journal of Microelectromechanical Systems* **2009**, *18*, 5 1100.

[77] G. Noh, S. Y. Yoon, S. Yoon, K. Kim, W. Lee, S. Kang, D. Lee, In *2016 IEEE/RSJ International Conference on Intelligent Robots and Systems (IROS)*. **2016** 3671–3676.

[78] D. Makarets, G. Noh, K. Kim, D. Lee, In *2014 14th International Conference on Control, Automation and Systems (ICCAS 2014)*. **2014** 217–220.

[79] C. Comte, J. von Stebut, *Surface and Coatings Technology* **2002**, *154*, 1 42.

Table of Contents (ToC)

This paper presents unprecedented miniaturized concentric tube robots (CTR) called Caturo, made of flexible glass tubes. The novel approach to obtaining different pre-curved tube shapes in glass involved thermal treatment using heat-shrink polymer and 3D printed mold. The process was characterized and the robot validated after which various demonstrations were carried-out to show its prospect in microsurgery.

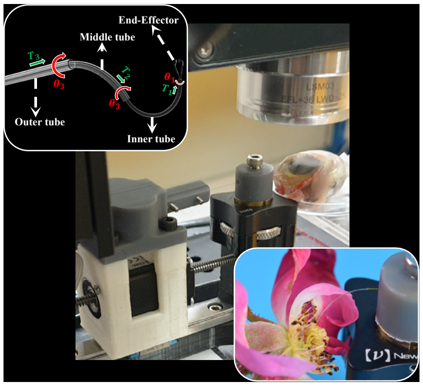

Miniaturized glass concentric tube robot for microsurgery